The CryoCapsule: Simplifying Correlative Light to Electron Microscopy

Xavier Heiligenstein[1,2,*], Jérôme Heiligenstein[3,4], Cédric Delevoye[1,2], Ilse Hurbain[1,2,5], Sabine Bardin[1,6], Perrine Paul-Gilloteaux[1,5,7], Lucie Sengmanivong[1,7,5], Gilles Régnier[3], Jean Salamero[1,5,7], Claude Antony[8] and Graca Raposo[1,2,5]

[1]Institut Curie, Centre de Recherche, Paris, 75248, France
[2]Structure and Membrane Compartments, CNRS UMR144, Paris, 75248, France
[3]Processes and Engineering in Mechanics and Materials, Centre National de la Recherche Scientifique (CNRS), UMR 8006, CER de Paris, Arts et Métiers ParisTech, Paris, France
[4]CryoCapCell, Paris, 75015, France
[5]Cell and Tissue Imaging Facility (PICT-IBiSA), CNRS UMR144, Paris, 75248, France
[6]Molecular Mechanisms of Intracellular Transport, CNRS UMR144, Paris, 75248, France
[7]Spatio-Temporal Modeling Imaging and Cellular Dynamics, CNRS UMR144, Paris, 75248, France
[8]Department of Structural Biology and Genomics, Institut de Génétique et de Biologie Moléculaire et Cellulaire, INSERM, U964, CNRS, UMR7104, Illkirch, BP10142, France
*Corresponding author: Xavier Heiligenstein, xavier.heiligenstein@curie.fr

Abstract

Correlating complementary multiple scale images of the same object is a straightforward means to decipher biological processes. Light microscopy and electron microscopy are the most commonly used imaging techniques, yet despite their complementarity, the experimental procedures available to correlate them are technically complex. We designed and manufactured a new device adapted to many biological specimens, the CryoCapsule, that simplifies the multiple sample preparation steps, which at present separate live cell fluorescence imaging from contextual high-resolution electron microscopy, thus opening new strategies for full correlative light to electron microscopy. We tested the biological application of this highly optimized tool on three different specimens: the *in vitro Xenopus laevis* mitotic spindle, melanoma cells over-expressing YFP-langerin sequestered in organized membranous subcellular organelles and a pigmented melanocytic cell in which the endosomal system was labeled with internalized fluorescent transferrin.

Keywords correlative light to electron microscopy, CryoCapsule, endosomal network, freeze substitution, high-pressure freezing, image registration, langerin, melanosomes, spatial resolution, temporal resolution, *Xenopus laevis* mitotic spindle

Received 28 August 2013, revised and accepted for publication 12 February 2014, uncorrected manuscript published online 17 February 2014, published online 24 March 2014

Correlative light and electron microscopy (CLEM) aims at bridging the time and resolution gap between light microscopy (LM) and electron microscopy (EM) (1–4).

A critical step in CLEM is the immobilization of the specimen between the LM and the EM. As EM for cell biology developed, chemical fixation was extensively investigated as an easy-to-use, affordable and time saving method for ultrastructure observation. But drawbacks inherent in the chemical fixation restrict the interpretation of dynamic events and their ultrastructure at the EM level in a CLEM perspective such as (i) the slowness of the sample fixation

(a few seconds to a couple of minutes depending on the specimen thickness and composition); (ii) the chemically induced ultrastructure modifications (membrane reticulations, ultrastructure reorganization, shrinking by dehydration and embedding of the specimen); (iii) the inefficiency of fixation for some specimens (*Caenorhabditis elegans* worms are motile for a couple of hours in 10% glutaraldehyde (2)); and (iv) the quenching of the fluorescence (5).

To preserve a sample's molecular and structural integrity, freezing methods have been developed to cryo-immobilize or vitrify specimens. Vitrification occurs within a few milliseconds and preserves a cell's ultrastructure (6). To date high pressure freezing (HPF) is the sole method allowing vitrification of samples from cells to small organisms (7–11). In HPF, the pressure is increased to 2100 bars and concomitantly the temperature is decreased to −196°C by liquid nitrogen within a 10 milliseconds timeframe. Under these conditions, the physical properties of water are modified, reducing ice nucleation during solidification by freezing (10) that preserves the cell ultrastructure in a 'close to native state' (8).

To establish a biologically meaningful CLEM workflow, dynamic fluorescent light microscopy must be rapidly followed by cryo-immobilization to proceed with EM (12). But high pressure freezing machines (HPM) are complex heavy machines (10,13) in which the HPF chamber, where the vitrification occurs is small, constrained and poorly accessible. To ensure proper specimen loading, multiple adaptors need to be assembled that delay the transfer, reducing the biologically relevant time scale of the CLEM method (http://www.youtube.com/watch?v=9kA2lswUpvw).
Accelerating and improving CLEM-HPF requires the development of tools that are compatible with the high-end LM standards, physically support the HPF process and facilitate the transfer of the specimen into the EM. Such tools will improve the temporal resolution between the last LM picture and the HPF (1,3) and guarantee high-end EM.

Three major HPM instruments are currently used among the cell biology community: the HPM010, the HPM100 and the EMPACT-1 and 2. The EMPACT-2 was designed to facilitate the rapid transfer from LMs to the HPF (3), but not all laboratories are equipped with this expensive equipment and mechanistic constraints of the EMPACT technology limit the sample size to less than 1.4 mm (3,13,14). In this article, we will refer to this machine as the EMPACT-2. On the other hand, the HPM010 can support specimens up to 2 mm in diameter while the HPM100 can use specimens up to 5 mm in diameter. As many laboratories are equipped with the HPM010 or the HPM100, a convenient tool is required to simplify transfer from LMs to the HPF of these two versatile machines. In this article, we will refer to these two machines as the HPMs.

We developed the CryoCapsule to accelerate, facilitate and standardize the sample manipulations throughout the CLEM workflow. We imaged our biological samples for 5 min before manual transfer from the light microscope to the HPM in a 15-second step. We reduced the non-thermoconductive mass to the minimum, therefore achieving cryo-immobilization in the culture medium without needing to add cryo-protectants (8,15) to preserve cell physiology. New HPMs adaptors were designed to prevent physical stress before vitrification. Finally, the shape of the CryoCapsule facilitates the handling steps for various specimens throughout the whole CLEM process until the targeted ultramicrotomy (1). The later stages of sample preparation are common to most EM approaches. We greatly simplified and accelerated the sample preparation process and increased the experimental reproducibility.

To challenge the CryoCapsule at the biological level, we tested three different samples: a fragile *in vitro* specimen, the *Xenopus laevis* mitotic spindle, described as pressure sensitive (16); melanoma cells (M10 cells) over-expressing a YFP-tagged Langerin that generated a membranous layered structure that is clearly visualized by EM (17); and a melanocytic cells line (MNT-1 cells) where we followed the endosomal network with fluorescent transferrin bound to endogenous transferrin receptors (18).

Results

The CryoCapsule: a new standard tool for CLEM in cell biology

The CryoCapsule is fabricated using over-molding technology. This process consists of injecting into a mold containing the inserts [the gold spacer ring and

the landmarked substrate sapphire disk (SSD)] a melted polyethylene polymer (PET) at high temperature and then letting it cool down and solidify. This industrial production method (19) ensures the complete reproducibility of the process and guarantees standardized production of the CryoCapsules (Figure 1). The final object is consistently of uniform dimensions (4.5 mm diameter, 0.6 mm thick, Figure 1A,D) and exhibits reproducible biophysical properties (sapphire disk, gold spacer ring and polyethylene plastic ring, Figure 1B). To our knowledge, gold and sapphire are not toxic to the cells. Although the release of PET phthalates is currently being investigated with respect to its impact on embryonic development (20). However, different cell types (MDCK, HeLa, MNT1 and M10 melanoma cells) grew normally and no increased cell death was observed.

The CryoCapsule is designed to simplify CLEM-HPF experiments. Therefore, we analyzed the thermal properties of the individual elements constituting the CryoCapsule. Sapphire disks of 50 µm have a cooling rate of 0.2 milliseconds (Figure S3) while rigid enough to avoid deformations or breakage during cryo-immobilization (depending on the HPM model, see below). Aclar® 33C Fluoropolymer sheets, often used as an alternative to sapphire disks (21,22) are flexible and have a longer cooling rate (23.3 milliseconds; Figure S3). We used 50 µm sapphire disks to guarantee the best cooling rate for the CryoCapsule. The gold spacer ring has a very fast cooling rate (0.02 milliseconds) and its height (50 µm) defines the CLEM chamber depth (Figures 1E–F and S3). The PET ring surrounding the CryoCapsule is not thermo-conductive and has a long cooling time (167 milliseconds; Figure S3), but is peripheral. Therefore it does not prevent the cooling of the sapphires and the subsequent cryo-immobilization of the biological specimen (Figures 3–5) in HPMs [as opposed to the EMPACT that separates pressure and cooling sources (13) as discussed below]. Finally, the water depth, defined by the height of the gold spacer ring, is the main thermo-resistant source (from 17.8 to 285.7 milliseconds; Figure S3). All together, the CryoCapsule is designed and composed of components supporting an optimal cryo-immobilization as required for CLEM-HPF.

In the live cell CLEM experiment step, carbon evaporated landmarks on the SSD (Figures 1B and 2B) (23) are used to locate the cells throughout the CLEM process (1). The substrate sapphire disk is inserted 275 µm deep into the CryoCapsule (Figure 1D), therefore long working distance objectives are required (Figures 1D–F and S2B). Industrial sapphire has a transmission range from 150 nm to 5.5 µm and a refractive index (RI) of $n = 1.67$. The commonly used fluorescent proteins have a working spectrum from 350 to 700 nm and the objectives are usually corrected for cover glass with a RI $n = 1.54$. Although sapphire is more refractive, we nevertheless obtained high quality fluorescence images, which were used to conduct the live cell imaging correlative experiments (see below Figures 4 and 5, Figure S1 and Video S1, Supporting Information).

The CryoCapsule simplifies both the specimen manipulation from LM to the HPM and the specimen embedding

Currently, most CLEM approaches using HPMs rely on a complex assembly of sub-elements appropriately superimposed in their respective adaptors before HPF. One possible assembly, derived from the work of Hawes et al. (15), is depicted in Figure 2C and Figure S1B. The total height of the two carriers (500 µm, type B) plus the two sapphire disks (50 µm) and the gold spacer ring (50 µm) generate an assembly of 1150 µm that needs to fit into the 1000 µm deep sample support (Figure 2F). Using this assembly, we noticed that the structure of a pressure-sensitive sample like the *in vitro X. laevis* mitotic spindle (16) was disrupted (Figure S1A–C).

Using the CryoCapsule prior to a CLEM-HPF experiment, a 2.5 mm diameter covering sapphire disk (CSD) is laid in the 2.8 mm CryoCapsule cavity (Figure 1D) on top of the gold spacer ring to close the isolating CLEM chamber where the sample is situated (Figures 1D–F and 2A, Video S2). Once the CLEM chamber is closed, all subsequent manipulations are done using the plastic ring (Figure 1B,C, Video S2). Moreover, the CryoCapsule is radially symmetric (Figure 1) to simplify the loading into the HPM holders (Figure 2D,E), and axially asymmetric (Figure 1) to facilitate the sample orientation upon embedding (Figures 1B and 2G).

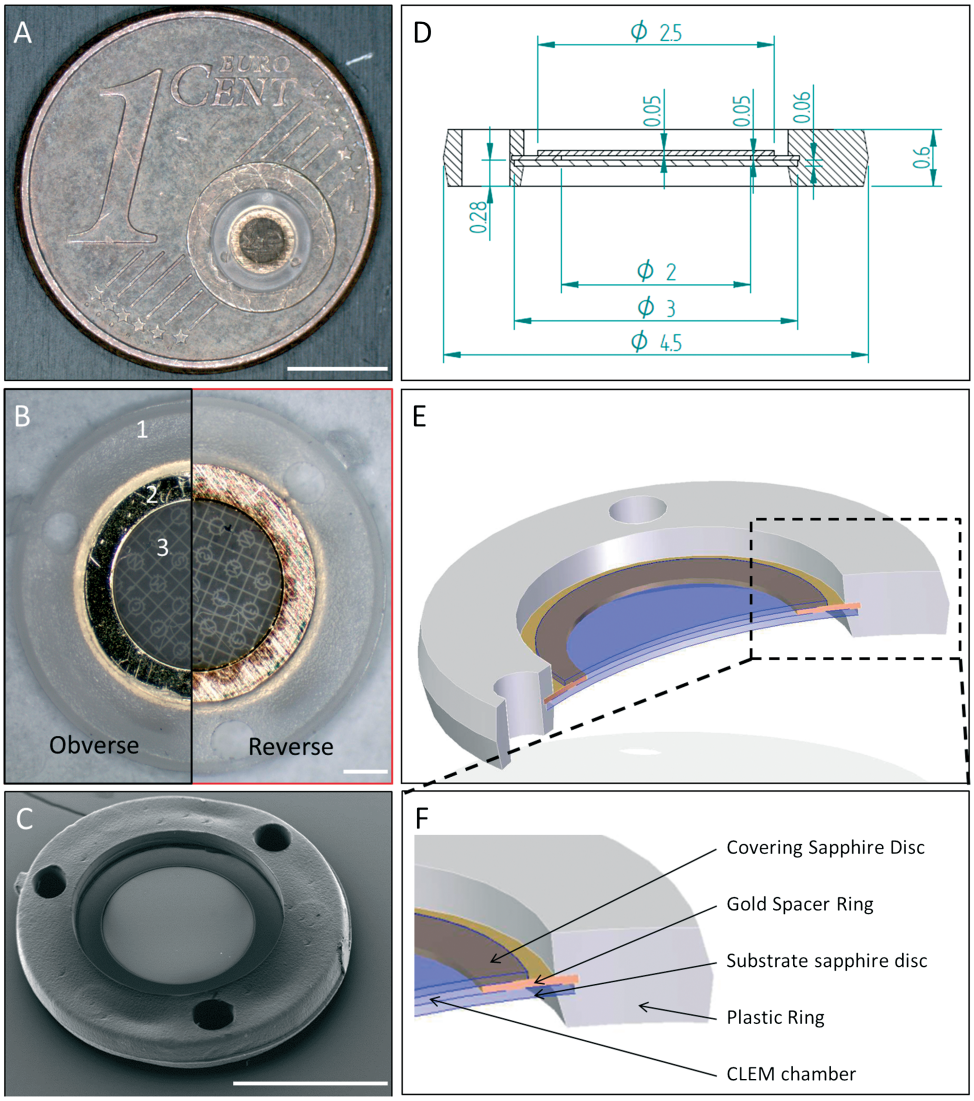

Figure 1: Detailed view of the CryoCapsule. A) Picture of the CryoCapsule on top of a 1 Euro cent coin, to illustrate the relative proportions; scale bar: 4.5 mm. Obverse (left) and reverse (right) magnified view of the CryoCapsule. Concentrically, the plastic ring (1), the gold spacer ring (2) and the landmarked substrate sapphire disk (3); scale bar: 0.5 mm. C) Scanning EM of the CryoCapsule; scale bar: 2 mm. D) Scaled side view of the CryoCapsule. E) Three dimensional cross section view of the CryoCapsule. The substrate sapphire disk and the gold spacer ring are embedded into the plastic ring and maintained together. The covering sapphire disk fit into the plastic ring and isolates the sample. F) Magnified three dimensional view of the CryoCapsule. The covering sapphire disk does not touch the plastic ring and lies on top of the gold spacer ring. Between the two sapphire disks and the gold spacer ring is the CLEM chamber.

We took into consideration the vitrification mechanism of both HPMs and developed two specific adaptors (Figures 2D,E and S2). They enable easier transfer of the CryoCapsule into the HPMs after live cell imaging as well as a decrease in the pressure on the specimen prior to HPF, minimizing pre-fixation stress (see below).

In the HPM010, vitrification occurs by direct impact of pressurized liquid nitrogen on the sample from both sides in the HPF chamber (24). We designed a clamp in which we removed the layer of aluminum on the SSD side as compared to conventional methods (Figure S2A) to obtain a direct hit of liquid nitrogen during

HPF on the SSD. To avoid deleterious shear forces or pressure applied to the specimen before vitrification, the CryoCapsule is maintained in the clamp by its plastic ring (Figure S2A). We tested the CryoCapsule by repeating the *X. laevis* experiment and observed no modification of the spindle assembly (Figure S1) indicating that the CryoCapsule preserves the structural integrity of wide and fragile samples.

For CLEM approaches, the CryoCapsule is placed in a humid chamber during live cell imaging (Figure 1D). Once the event of interest has been identified, the CryoCapsule is mounted in the HPM010 clamp for HPF (Figures 1D and S2A). The transfer operation takes approximately 30 seconds depending on the user's skills.

In contrast to the HPM010, in the HPM100 the liquid nitrogen comes as a side flow, so we left a direct exposure

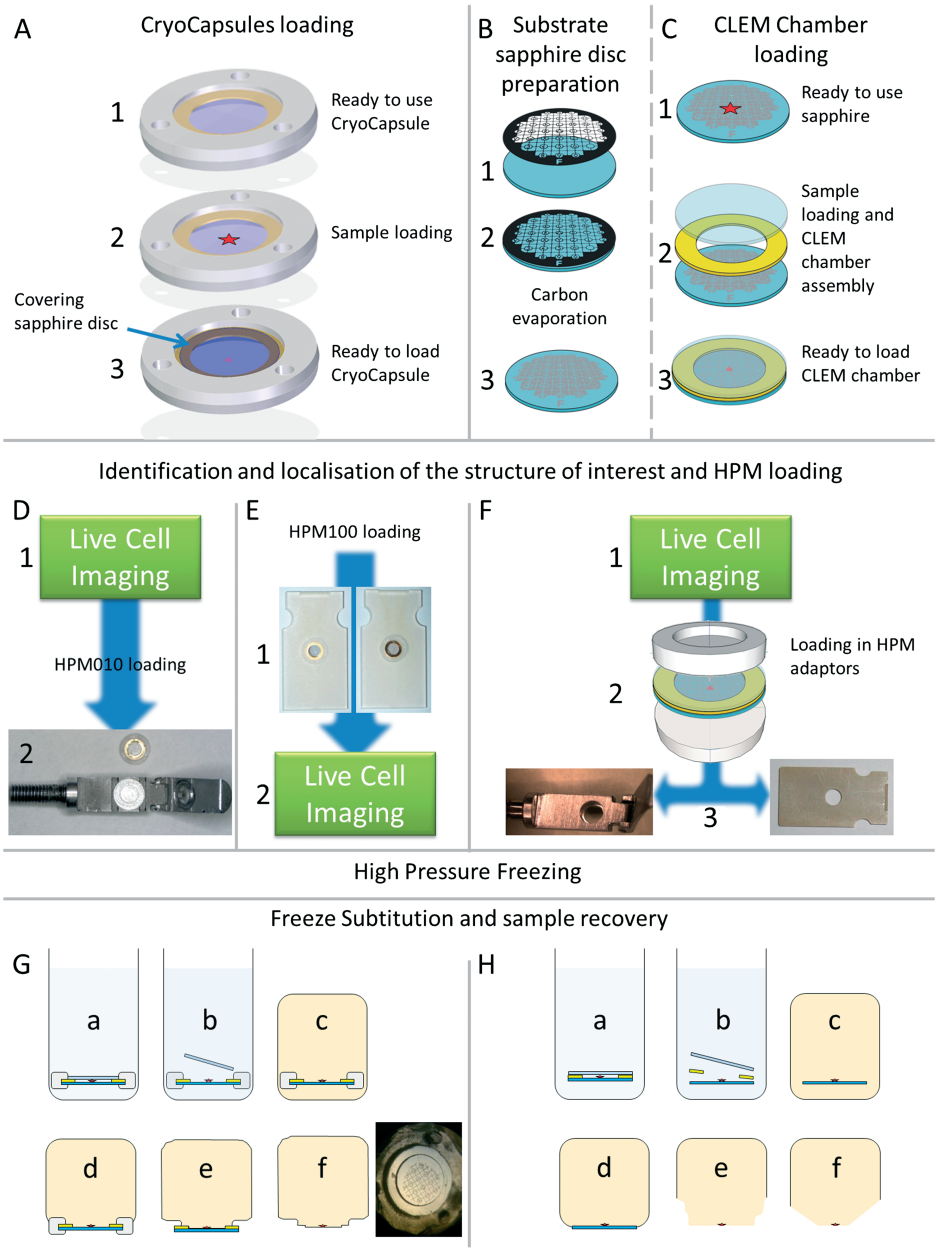

Figure 2: Legend on Next Page.

of the sapphire disk to the LN2 from both sides. After deposition of the CSD to close the CLEM chamber, the CryoCapsule is clipped in the middle plate adaptor that we specially designed and produced (Figure 2E, Video S1, S2). The CSD is maintained in place by a lip and the whole assembly stays clipped (Figure S2B, Video S1, S2) unless an external force is applied. For CLEM approaches, the assembly of the CryoCapsule and Adaptor is imaged in a humid chamber. After identification of the event of interest, manual transfer is performed in approximately 15 seconds according to the user's skills, and is therefore suitable to study cell processes happening within a timeframe of at least 20 seconds (See below Figure 5, Video S2).

The EMPACT high-pressure freezer uses a fundamentally different mechanism to manipulate and cryo-immobilize the specimen (13). The cooling, separated from the pressure source, comes to the side of the specimen (13) and the CryoCapsule is surrounded by a thermo-resistant polymer. We expect the plastic ring to prevent proper cooling of the specimen, hence cryo-immobilization. Furthermore, a rapid transfer system (RTS) has already been developed for the EMPACT-2. Thus we only tried the compatibility of the CryoCapsule with HPM010 and −100.

Using both HPMs, the manipulations are reduced to: (i) placing the CSD, (ii) loading the closed CryoCapsule in the HPM adaptor, (iii) vitrifying. At no time is the specimen exposed to external shear forces or pressure as all the manipulations are done via the plastic ring. Altogether, the CryoCapsule is compatible with both HPMs.

High-pressure freezing using the CryoCapsule preserves cell morphology

To validate the vitrification efficiency of the CryoCapsule we tested different cell lines using both HPMs (Figure 3).

After sterilization in 70% ethanol, the capsules were placed in culture Petri dishes, allowed to dry for a couple of hours and then HeLa cells, MDCK or MNT1 and M10 melanoma cells were plated (Figures 3 and 4).

Generally five CryoCapsules are prepared per HPF experiment. MDCK cells were vitrified with an HPM010 using hexadecene as a filler to reduce the water content (Figure 3A; 8), MNT1 cells were cryo-immobilized

Figure 2: The CryoCapsule is an integrated technology that simplifies the manipulation of biological specimen in HPFCLEM approaches. A) Schematic views of the CryoCapsule in use: the substrate sapphire disk of the CryoCapsule is already landmarked by carbon evaporation through a finder grid mask. After sterilization (1) for an experiment, the specimen (red star) is loaded (2) and a 2.5-mm diameter covering sapphire disk (blue arrow) is deposited to encapsulate the specimen (3), creating a CLEM chamber. B) Carbon evaporation process used in both the CryoCapsule and the conventional CLEM approaches. A finder grid is deposited onto a substrate sapphire disk (1, 2) and carbon is evaporated through it, creating a negative mask to localize the samples of interest throughout the CLEM process (3). C) Possible sapphire assembly for correlative approaches: a biological specimen is deposited onto a landmarked substrate sapphire disk (1), a spacer ring (2) is laid on top of it followed by a 3 mm diameter covering sapphire disk (3). D–F) After assembly of the CLEM chamber, the specimen is prepared for live cell imaging to identify a structure of interest prior to HPF. D and E) The CryoCapsule is loaded into a bottom-perforated humid chamber for direct imaging using a long working distance objective (1). After identification of the sample, the CryoCapsule is collected and mounted into the HPM010 tip (2) for HPF. E) The CryoCapsule is clipped into the HPM100 middle plate adaptor (1; Pictures of the obverse and reverse sides of the loaded adaptor). F) The sapphire assembly is imaged in a glass bottom humid chamber (1) to identify the region of interest. The assembly is mounted between two aluminum carriers (2) and loaded into the HPM adaptors before HPF (3). G) The CryoCapsule is transferred into the freeze-substitution solution (a) and the covering sapphire disk is gently removed, manipulating only the plastic ring and the covering sapphire disk (b). The orientation is done reading the carbon letters or facing the gold spacer ring up (c). After embedding, the removal of the soft plastic ring (d) leaves the sapphire disk accessible for a careful physical removal (e; no heat shock required). The carbon pattern transfers to the resin for a facilitated targeted ultramicrotomy (picture). H) The sapphire assembly is transferred into the freeze-substitution solution (a) and disassembled to collect the substrate sapphire disk (b). Orientation of the sample is done exclusively by reading the carbon letters (c). After embedding, the sapphire disk is cleared (d) and removal is done using heat shock or mechanical removal (e). The carbon pattern transfer is used for targeted ultramicrotomy (f).

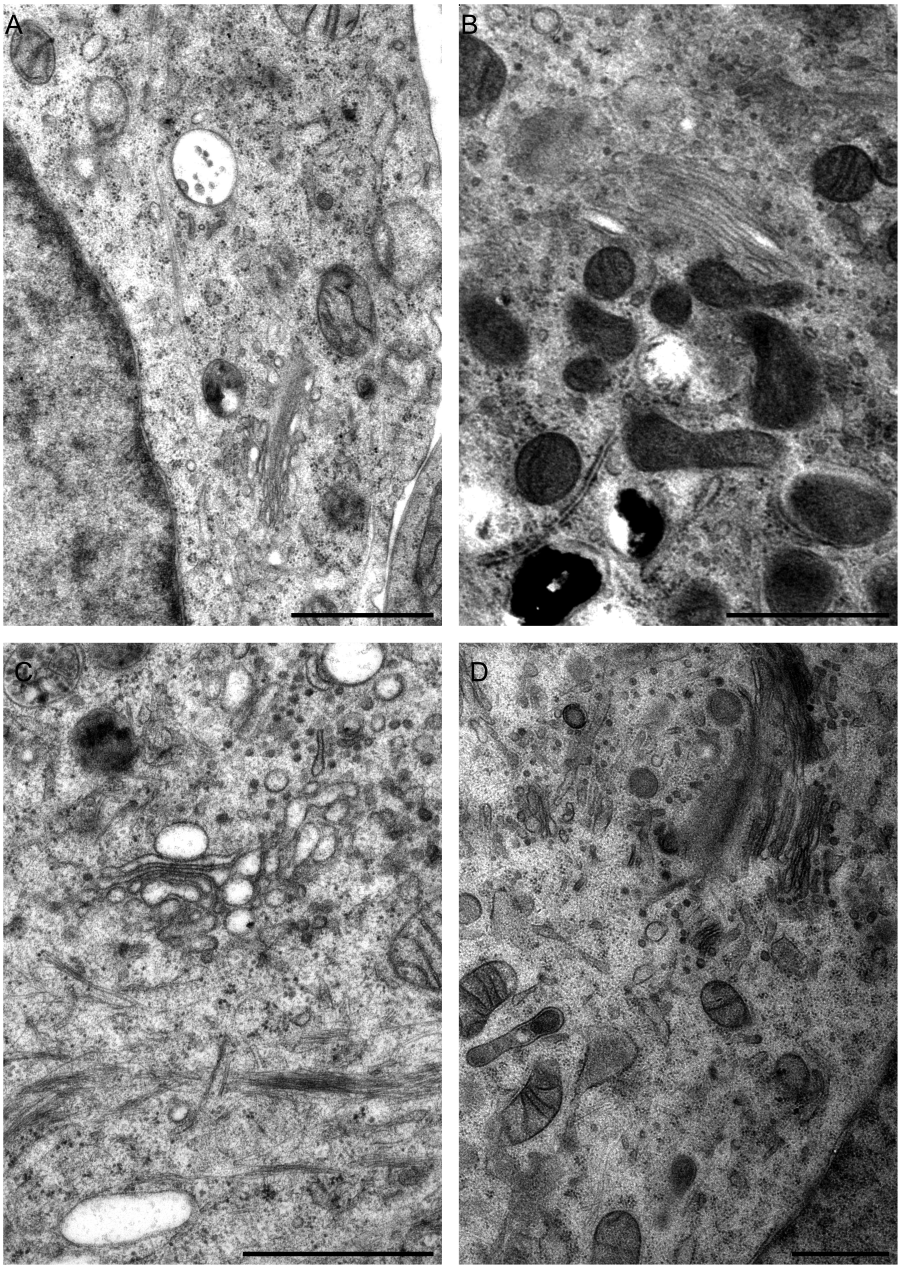

Figure 3: The CryoCapsule allows the vitrification of a large range of cell lines with both the HPM010 and the HPM100. A) MDCK cells were vitrified using hexadecene as medium filler in a HPM010, FS: 0.1%uranyl acetate, 0.2% glutaraldehyde and 2% H_2O in dry acetone. B) MNT1 cells were vitrified in an HPM100 in their culture medium without cryo-protectants or filler, freeze-substitution: 0.1% uranyl acetate, 0.05% glutaraldehyde, 1% H_2O in dry acetone. C) HeLa Kyoto cells were vitrified in a HPM010 without cryoprotectants or filler, freeze-substitution: 0.1% uranyl acetate in dry acetone. D) HeLa Kyoto cells were vitrified in an HPM100 without cryo-protectants or filler, FS: 0.1% uranyl acetate in dry acetone. Scale bar = 10 m.

on a HPM100 in culture medium containing HEPES (Figure 3B) and finally HeLa cells were cryo-immobilized in culture medium. In each case the experiments were repeated using both HPMs (Figure 3C,D). M10 Melanoma cells were also cryo-immobilized, using a HPM100, in culture medium containing HEPES (Figure 4). In all cases, the ultrastructure of the cells was well preserved without any detectable segregation artifacts (ice patches, broken membranes). The cytoplasm was homogeneous and the Golgi apparatus, the nuclear membrane and the mitochondria were well preserved (Figure 3). Overall, the CryoCapsule is compatible with cell cultures and preserves the ultrastructure of high pressure frozen cells without the use of cryo-protectants.

CLEM with the CryoCapsule

Mainly two different approaches exist to achieve CLEM. With the first, the specimen is imaged live, fixed and the cell of interest is recovered in the EM. This method is often applied to time-lapse studies or to narrow down to the cell

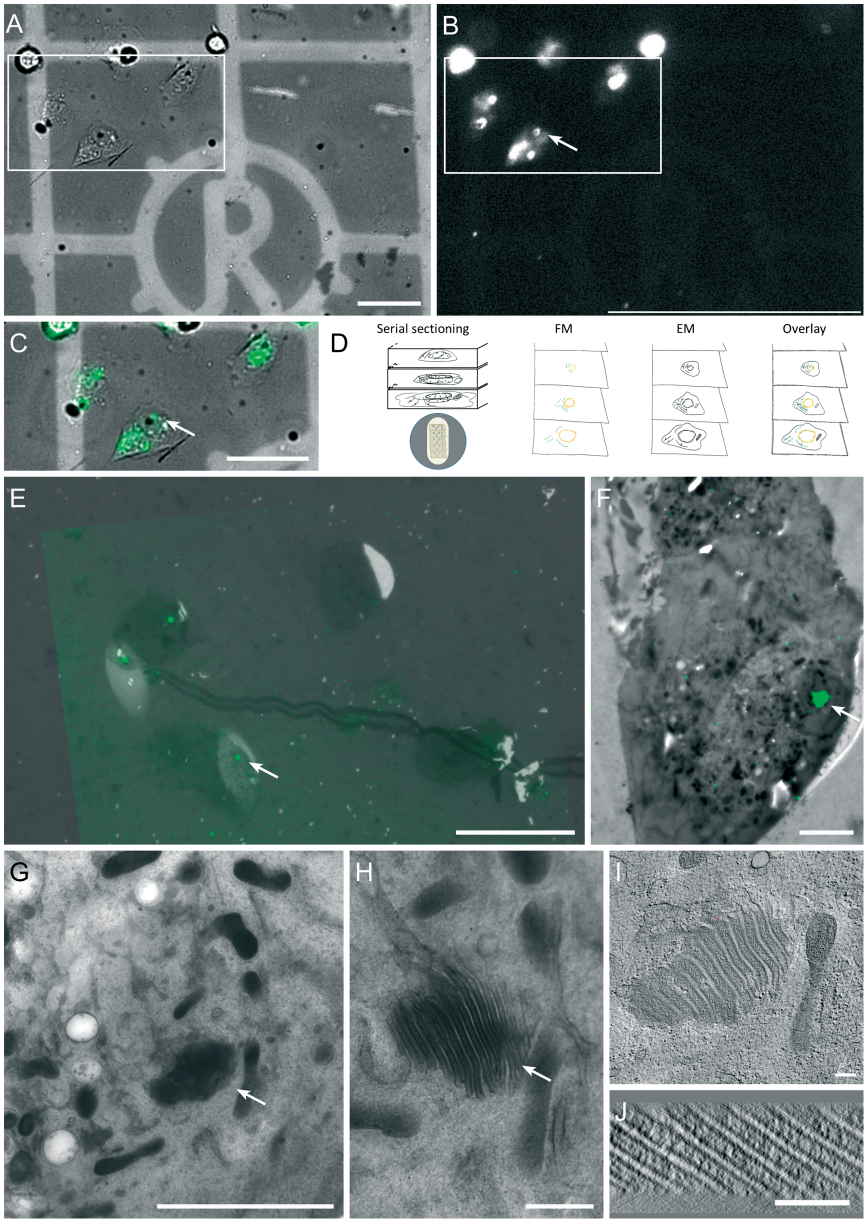

Figure 4: Full CLEM workflow. A) The cells (arrow head) in the CLEM chamber are localized at the surface of the substrate sapphire disk using the carbon landmarks; scale bar: 50 μm. B) The cells of interest (YFP-langerin stably expressed in M10 melanoma cells) are identified in fluorescent channel (arrowhead); the fluorescent signal of the OSER is voluntarily saturated for illustration purpose and is indicated with a white arrow; scale bar: 50 μm. C) Magnified overlay of the cell of interest (dashed line A,B); scale bar: 50 μm. D) Schematic representation of the sample preparation for the second imaging step: the cells are serial sectioned (250 nm thick) and collected on slot grids. Each individual section is imaged by bright field and fluorescence light microscopy then imaged by EM, and finally overlaid. E) Affine overlay is done with very low magnification image (540×) and used to locate the OSER within the cells (arrowhead); scale bar: 50 μm. F) Low magnification (2400×) picture of the cell is overlaid with the former overlay (E) to locate the OSER (arrowhead); scale bar: 5 μm. G) Medium magnification image of the OSER (arrowhead); scale bar: 5 μm. H) High magnification tilted EM (−54°) acquired on a 200 kV EM: the layered structure is clearly identifiable (arrowhead); scale bar: 1 μm. I) Electron tomogram top view slice of the OSER showing a clear layered organization; scale bar: 0.2 μm. J) Electron tomogram cross view of the OSER (along the yellow line in I); scale bar: 0.2 μm.

of interest from a population of cells (1,25). The second approach consists of cryo-immobilizing the specimen and then imaging the fluorescence directly on the EM sections prior to EM imaging. Using landmarks on the sections, the structure of interest is accurately localized (below 100 nm precision) on a physical slice of the cell (26).

The CryoCapsule allows combination of these two approaches into a full CLEM workflow where one can monitor and image the sample between each processing step. We used M10 melanoma cells stably expressing YFP-tagged langerin (the component of the Birbeck granule of Langerhans cells) in its cytoplasmic domain (YFP-langerin) (17). These cells exhibit a very bright fluorescent signal, easy-to-detect by light microscopy at low magnification [10× or 40× air extra-long working distance (ELWD) objectives] (Figure 4, Video S1). In these cells, the YFP-langerin accumulates into organized smooth endoplasmic reticulum (OSER)-like structures (17). These structures correspond to regions of the ER where the YFP-langerin accumulates by dimerization of the YFP, trapping the fluorescent signal in large layered compartments that also share common morphological features with Birbeck granules (17). At the EM level, these layered membranous structures sequester the heavy metal salts used to contrast the specimen and are clearly identifiable electron dense and organized regions (Figure 4G–J) (17).

After identification of the cells of interest by live cell imaging and their localization using the carbon pattern (Figure 4A–C, Video S1), the cells were cryo-immobilized in a HPM100 followed by freeze substitution (FS; Figure 4A, Video S1). As we also planned to do fluorescence imaging on these sections, the cells were embedded in HM20-Lowicryl with low a fixative concentration to preserve the fluorescence of the tagged proteins (5,27). The CryoCapsule was extracted from the adaptor directly into the FS solution at −90°C; the removal of the CSD was carried out by simply lifting the CryoCapsule to the side and letting the CSD fall off by gravity (Figure 2G). PET is not dissolved by acetone; hence the entire structure stands as a whole assembly until embedding in Lowicryl. After polymerization, the PET ring is removed using a razor blade and the SSD is gently mechanically removed. The carbon landmarks transfer to the Lowicryl bloc, allowing a precise targeted ultramicrotomy (Figure 2G). Serial sections (300 nm in Figure 4 or 100 nm in Video S1) are collected on slot grids and imaged by fluorescence and transmitted light microscopy (Figure 4D). The sections are not flat on slot grids, so a Z stack is acquired to collect the entire fluorescent signal. Lowicryl is a rather soft embedding resin and uneven UV polymerization leads to small imperfections in the bloc. Tiny holes appear on the plastic sections that diffract strongly in transmitted light, inverting from black to white according to the focal plane. These imperfections were used as 'natural landmarks' to register the fluorescence in the EM images where the same holes appear white (Figure 4E). Although not as precise as the fluorescent fiducial markers used by Kukulski et al. (27), they are sufficient to accurately locate the OSER signal within our cells (Figure 4, Video S1). Registration was performed using the plugin TurboReg (28) in Fiji. The calculated affine deformation from the transmitted light image was applied to a Z-projection of the fluorescent stack after background removal and then overlaid with the EM image at very low magnification (Figure 4E, Video S1). This mapping is then used to retrieve the fluorescent signal within the cell (Figure 4F, Video S1), acquire tilt series images to observe the layered structures described previously (17) and reconstruct electron tomograms of the OSER (Figure 4G–J). This indicated that the specimen cryo-immobilized with the CryoCapsules were equally well preserved as other cell monolayers using HPF approaches and that the CryoCapsule is suitable for a full CLEM approach.

The M10 melanoma cells that we used to set-up the workflow express an unusually high level of fluorescence and the OSER structures are rather immobile. We aimed to further challenge the use and benefits of the CryoCapsule to overcome the technical limitations of the HPM transfer systems. With this concern in mind, we investigated the dynamic interactions between the endosomal and melanosomal network of pigmented melanocytic cells. Previous studies from Delevoye et al. (18) have shown that in MNT1 cells, endosomes followed with internalized fluorescent transferrin (Tf) interact transiently with melanosomes (∼20 seconds) (18). To track the endosomal network and accurately identify it near melanosomes we acquired wide field images for 3′20″ by bright field and fluorescence microscopy every 25 seconds with a 40× air objective (Figure 5A). At the top left of the cell,

we selected a group of melanosomes (Figure 5A, black arrowhead) apposed to Tf-positive endosomes (Figure 5A, red arrowhead) at the end of the imaging period (2′55″ and 3′20″, insert box). The Tf-fluorescent signal, slightly below the melanosomes (Figure 5B), has an elongated form with a brighter signal toward the bottom (Figure 5B, inserts). Then we manually transferred the CryoCapsule into the HPM100 for cryo-immobilization in less than 15 seconds and processed it for EM (Video S2). We imaged all the fluorescence on the section on the day of sectioning, since fluorescence is rapidly quenched after sectioning (less than 24 h). As the Tf-A555 is internalized by binding to the endogenous pool of Tf receptors, the intensity of the fluorescent signal is rather low. This second step of light imaging was performed using a 60× oil objective with a numerical aperture of 1.4 in order to easily detect the fluorescence on the EM sections and increase the fluorescence-localization accuracy.

The image alignment was carried out following the same procedure as described previously but using the black pigmented melanosomes as natural landmarks instead: they are easily distinguishable by bright field imaging even on EM sections. The cell shape and the melanosomes are also used to correlate the live cell imaging with the EM sections. The overview of the cell, taken at low magnification by EM (Figure 5C) displays a comparable distribution of the melanosomes at the cell periphery. The first 13 serial sections (200 nm each) imaged both by LM and EM and registered for fluorescence were aligned manually with each other with MIDAS (29) to reconstruct part of the endosomal–melanosomal network (Figure 5E–G). Fluorescence of the section aligned with the EM (Figure 5D) allows one to identify the labeled endosomal network (Figure 5D, red arrow) apposed to melanosomes (Figure 5D, black bow) from other tubular structures. The melanosomes were concentrated in the bottom three serial sections (Figure 5E–G). Tubular endosomal structures expand across the three sections and the intensity is brighter toward the bottom (Figure 5G) as observed by LM (Figure 5B). Taken together our data show that the CryoCapsule enables a full CLEM approach on either static fluorescently labeled structures or highly dynamic endosomal tubules that can be followed with a low intensity fluorescent signal, adequate for broad cell biology approaches.

In conclusion, and as compared to the currently available tools and methods, the CryoCapsule simplifies the sample handling from the cell culture step and the sample loading until the targeted ultramicrotomy (Video S2). This simplification allows us to track and image the specimen at almost every processing step, ensuring a reliable integrative full CLEM analysis of dynamic biological process (i.e. within a timescale not less than 20 seconds).

Discussion

CLEM is not only regarded as a powerful and straightforward method for cell biologists, but it is also considered technically challenging. The handling of the specimen is often complex and requires careful adaptation to each biological object (4,14,25,27,30). Generally, vitrification by HPF of cell suspensions has a success rate of approximately 80% using cryo-protectants (8). Live CLEM approaches require identifying the specimen before HPF and retrieving it after sample processing for EM (1,3,31). The handling complexity of the specimen dramatically reduces the success rate for each experiment.

We created the CryoCapsule to provide a robust and reproducible approach to perform CLEM, while minimizing the external stress factors that could influence the interpretation of the experiment. Hence we addressed the sample manipulation, the cell culture and imaging settings, the fixation conditions, the live imaging time and the dimensions of the sample.

For most studies on cell lines, the cells are cultured on 50 µm thick sapphire or Aclar®33C disks (22,23). Often, the transfer from the light microscope to the HPM is a source of stress for the cells. Disks of 50 µm thickness are difficult to handle with tweezers and can be dropped, inducing dehydration of the specimen thus damaging the cells before cryo-immobilization. Furthermore, assembling several small independent parts (B carriers, spacer rings) takes a significant amount of time and skill. This hinders conducting fast correlative experiments, increases the risk of damage to the cells of interest and limits routine use of CLEM on HPMs. The CryoCapsule includes the elements commonly used in CLEM approaches and hold them in a single unit, reducing the handling to a single element. Moreover, the size and

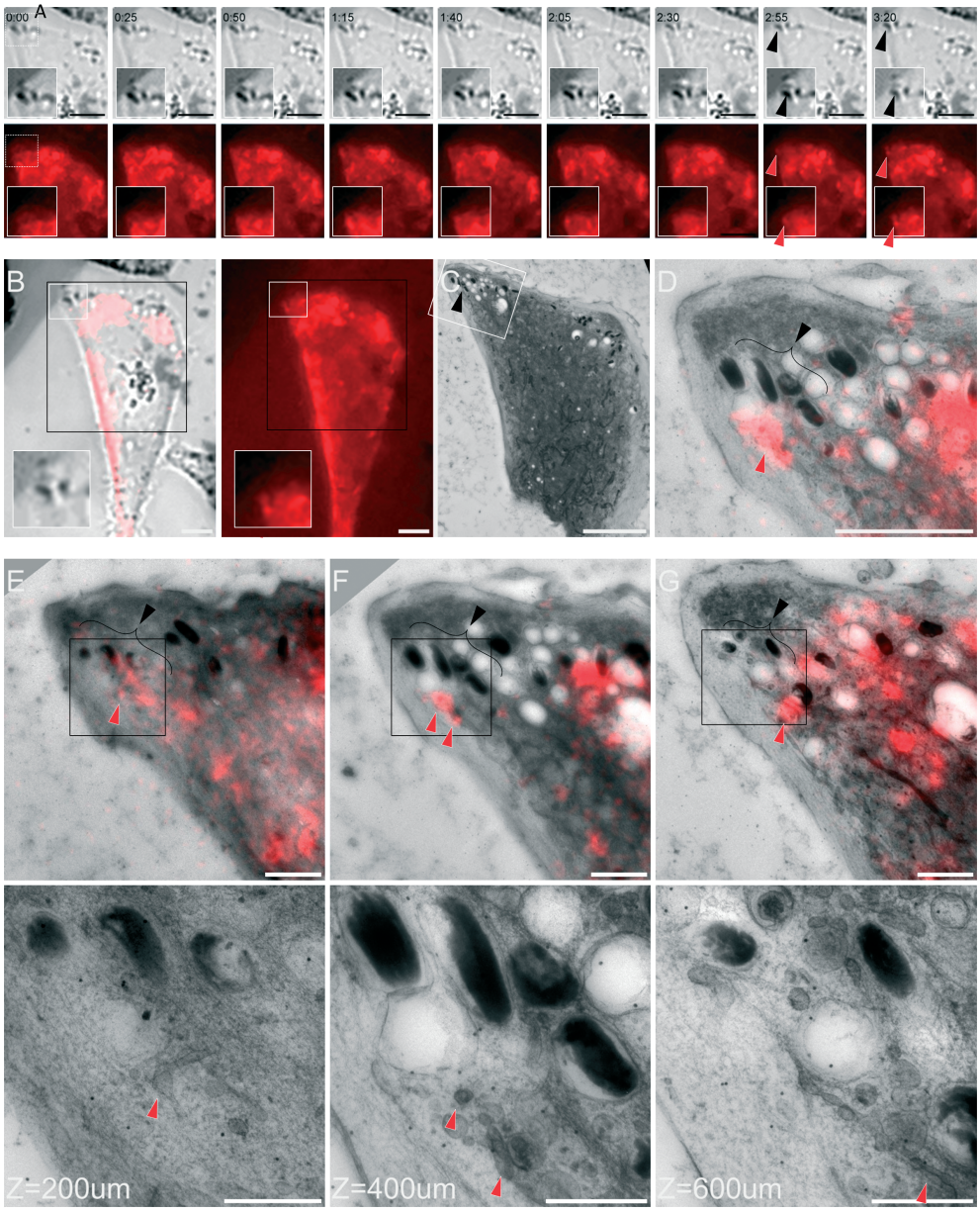

Figure 5: Correlative microscopy of the endo-melanosomal dynamic networks' interactions. A) MNT-1 cells were imaged by transmitted and fluorescence light for 3′20″ before a rapid transfer into the HPM100 for cryo-immobilization. In the last two frames, a Tf-positive endosomal structure of tubular appearance (red arrowhead) was observed close to the melanosomes (black arrow head) and was targeted for correlative imaging; the boxes are magnified views of the dashed white box (first frames); scale bar: 50 μm. B) Overview of the MNT-1 cell at the last time point before cryo-immobilization; the black box represents the field of view covered in (A) and (C). The Tf-positive tubular structure (red arrowhead) in the white box is slightly below the melanosomes (black arrowhead); the white box corresponds to the magnified field of view in (A) and (C)–(G); scale bar: 50 μm. C) Low magnification EM of the cell of interest. The white box delimits the region of interest, the black arrowhead points the melanosomes; scale bar: 50 μm. D) Overlaid magnified view of the white box (A–C); the melanosomes (black bow) are above the endosomes (red arrowhead); scale bar: 20 μm. E–G) First three sections containing biological material, $Z = 200$ nm, 400 nm, 600 nm. The melanosomes (black bow) and the endosomes (red arrows) are observed; scale bar: 10 μm. Below are the magnified views of the black boxes. Scale bars: 0.50 μm.

shape of the CryoCapsule facilitate the manipulations in the various confined environments inherent to EM (HPF, freeze-substitution, ultramicrotomy). The simplified handling avoids the addition of undesired stress on the specimen, improving the reproducibility of each experiment.

Compared to a naked sapphire disk supporting the cells, orientation of the specimen in the FS media is significantly improved, reducing the risk of damaging the cells with tweezers. Last but not least, determining how best to orientate the SSD in the freeze-substitution automate is straightforward (Axial asymmetry of the CryoCapsule, Figure 1B).

The design of the CryoCapsule also allowed us to cryo-immobilize the cells in their culture media (15) (Figure 3). Often in HPF, the use of cryo-protectants such as BSA 20%, Dextran 40 KDa 20% or filler like hexadecene is advised to improve the success rate of vitrification (8,9,32,33) but these components introduce the cells to non-physiological conditions. As cryo-immobilization by HPF aims to preserve the ultrastructure as 'close to native state' as possible, the adjunction of cryo-protectants may stress and influence cell ultrastructure.

To investigate the consequences of physical stress applied to the specimen prior to HPF, we used the *X. laevis* mitotic spindle and simulated its immobilization by HPF. *X. laevis* mitotic spindle has been described as sensitive to pressure and shear forces (16). We loaded the specimen in the CryoCapsule, closed the HPM010 clamp and transferred the clamp with the enclosed CryoCapsule into the HPM chamber but did not proceed to HPF (Figure S1D,E). The sample was recovered and imaged again under the same light microscope. We observed a moderated specimen shift with regard to the carbon landmark used to localize and identify the mitotic spindle (Figure S1F). We assume this shift is the consequence of the dynamic instability of the microtubules that locally adhere to the substrate, inducing displacements of the structure. If shear forces or pressure were applied they were not sufficient to disassemble the spindle (16).

Using HPF, the main limiting factor to vitrification itself is the water content of the specimen (Figure S3). Although our experiments show that we can cryo-immobilize many cultured cells without cryo-protectant, all cell types show different requirements for vitrification and we cannot exclude the need for cryo-protection in some cases. Also, with deeper CryoCapsules, cryo-protection might be required. Combining the limited physical stresses and cryo-immobilization in growth media, the specimens are kept very close to native state until cryo-immobilization. The observations done at EM level are hence very comparable to their 'native state'.

Once cryo-immobilized, the sapphire disk in the CryoCapsule prevents performing cryo-sectioning and evaluating a 'vitreous state'. We used the cell morphology to evaluate the fixation quality.

To conduct live cell imaging in the CryoCapsule, we added HEPES to the culture medium as our stage controls the temperature but not CO_2. When the experimental temperature was maintained at 37°C, a progressive evaporation occurred causing the appearance of air bubbles after 6 or 7 min of observation. As well as the deleterious dehydration of the specimen, air bubbles, even tiny, prevent the raising to full pressure in the sample chamber (compression of the gas) compromising proper cryo-fixation. Hence we kept the imaging time within 5 min. In this time frame, experiments were successful. For longer experiments, further adaptation and developments will need to be implemented.

The newly developed CryoCapsule is 50 µm deep, limiting its use to cell cultures or very thin specimens. In the future, thicker spacer rings will be available to use depending on the biological requirements, e.g. tissues, up to the vitrification's physical limit of 300 µm. The imaging window width is 2 mm. Although for many cell biology experiments it might be sufficient, some specimens might require a larger support. We evaluate the feasibility of using a 5-mm imaging window CryoCapsule based on the 6 mm sapphire disks that is used on the HPM100. The larger size of this CryoCapsule opens possibilities to using immersion objectives (as discussed below).

Correlative microscopy for HPMs as we described here relies on two fluorescent imaging phases: first, the cells are imaged live before HPF. So far in this first phase, most approaches are based on live cell imaging on a substrate

supported in a Petri dish surrounded by culture medium. In that case, the light path goes through a first diffraction barrier of the Petri dish glass bottom (RI: $n \sim 1.52$) and the liquid phase of the culture medium (Water: $n \sim 1.33$), the substrate support (Sapphire: $n \sim 1.67$; Aclar: $n \sim 1.45$) before reaching the specimen. As none of these materials have the same RI, the light path is strongly perturbed reducing significantly the detection level. The EMPACT-2 recently circumvented these constraints with the inverted RTS set up (34). For the HPMs, the CryoCapsule as a standalone element, permits direct imaging through the sapphire substrate, removing at least one phase transition. The current use of air objective (Air: $n = 1$) is not optimal and the 6 mm CryoCapsule should allow the use of immersion objectives to improve significantly the light sensitivity.

Bearing in mind all these technical considerations, we analyzed two different types of samples in the CLEM method presented here. First, the M10-11G provided an ideal cell model to set-up the workflow because of their very bright and stable fluorescent signal (17); long working distance objectives were used because fluorescence was not a limiting factor. Setting up this method, we decided to use the same light microscope in every fluorescence step to obtain directly comparable images. As we aimed for a rapid transfer of the specimen from the light to the EM, the use of immersion objectives was avoided for two reasons: (i) Oil is thermo-resistant and requires solvents to be efficiently removed and so is inappropriate for 'live cell' CLEM. Water is also a thermo-resistant although blotting would be possible, but prevents a rapid transfer. (ii) The shape of the actual CryoCapsule leads the SSD to be 275 µm deep in the CryoCapsule. So a water immersion objective with at least 300 µm working distance would be necessary. Considering the very bright signal and large stable structures of interest in our specimen, we estimated the use of 10× or 40× for live cell imaging to be sufficient for setting up our method. For the fluorescence on sections, the method described by Kukulski et al. (27) uses a 100× oil immersion objective on single sections. We optimized our method for a full cell correlative approach, where we image the fluorescence on every section across 50 serial sections, sometimes imaging several cells on each section. As the fluorescent signal is very bright and our initial aim was not to image small subcellular structures, a broader field of view was more convenient and facilitated the localization of the cells on each section.

Although we used the first cell system to more easily establish the set up, our goal was to be able to image highly dynamic structures. The second sample we analyzed was more challenging with respect to its dynamic nature and the fluorescence intensity levels. We followed smaller subcellular structures, such as endosomes, that can be labeled with an internalized fluorescent ligand bound to a pool of endogenously expressed receptors. The early endosomal network in MNT-1 cells is composed of vacuolar endosomes and 70 nm wide endosomal tubules that can extend over a micrometer in close proximity to pigmented melanosomes (18). We used the 40× air objective for live cell imaging for the reasons already stated above. But a better detection of the fluorescence across several sections was necessary to investigate this complex network. Using a 60× oil immersion objective, the signal sensitivity and the localization were significantly improved opening post-processing image analysis solutions going toward super-resolution imaging (35) while keeping a reasonably large field of view, helping to orient the specimen. Last, for this second sample, we used a protein coupled to Alexa-555 and we were able to detect a bright fluorescent signal. We are not aware of another publication reporting the efficiency of this fluorophore after HPF so it adds to the growing list of fluorescent labels that can be used for correlative experiments.

As CLEM grows more important for biological analysis, the CryoCapsule is a novel tool that simplifies the sample preparation and manipulation along the several steps required for CLEM. One potential application is for the cryo-CLEM, observing the vitrified cells in a cryo-stage for later super-resolution microscopy approaches (after vitrification, in cryo-stages).

Materials and Methods

Cell culture

The CryoCapsules (CryoCapCell) were stored for 72 h at +60°C to harden the carbon layer, sterilized in 70% Ethanol a day in advance and left to dry in the petri dish where the cells were plated.

HeLa Kyoto cells were grown in 4.5 g/L glucose DMEM (Gibco), 10% fetal calf serum (FCS), 1% penicillin/streptomycin, 1% glutamine and plated into the CryoCapsules 2 days before HPF.

MDCK cells were cultured to confluence in MEM supplemented with 10% FCS and plated onto the CryoCapsules 2 days before HPF.

M10-11G cells were cultured in RPMI 1640 (Gibco), 10% FCS, 0.5% geneticyn (Gibco) for 2–3 days before vitrification to ensure good attachment of the cells. Cells were grown so they would grow separately to simplify the cells identification and location in CLEM experiments.

MNT-1 cells were cultured in DMEM, 4,5 g/L glucose, 20% FCS, glutamine, penicillin, streptomycin, for 3 days before HPF. Cells were not grown to confluence. For the CLEM experiment, the cells were starved for 1 h and incubated with Alexa-555-labeled Tf (Tf-A555 10 µg/mL) for 30 min prior to live cell imaging.

In vitro mitotic spindle preparation and imaging

The mitotic cytostatic factor free spindles were assembled *in vitro* according to the procedure first described in (36). They were directly pipetted into the CryoCapsules without pre-treatment. The spindles were imaged on a Zeiss Axio Observer Z1 (Zeiss), with a 20× LD plan-NeoFluar (NA 0.2; WD 8.5), LED module 540–580 nm.

High-pressure freezing

Validation of cryo-immobilization was done on a HPM010 (Abra Fluid) at ABRA FLUID AG, Widnau, Switzerland. The correlative approach plus cryo-immobilization validation was done on a HPM100 (Leica Microsystem), Institut Curie, Paris France.

Sample orientation of the specimen during FS

After cryo-immobilization, the specimens are freeze substituted with Lowicryl (HM20) in an AFS-2 for further analysis by EM. In the freeze-substitution solution at −90°C, the CSD is gently removed and the CryoCapsule orientation is elucidated by reading the carbon pattern from the SSD, manipulating exclusively the plastic ring and thus avoiding tweezers manipulations damages to the sample (Figure 1G). Conveniently, the CryoCapsule fits in the Leica flow-through chambers so samples, once oriented, can be deposited at the bottom and embedded in a similar manner to other HPF samples.

In comparison, the sapphire assembly (Figure 1C) tends to dismantle in the FS solution (Figure 1H), sometime damaging the specimen and adding complexity to the sample orientation for embedding.

FS and sectioning

Freeze-substitutions were performed in an AFS-2 from Leica Microsystem. Samples were kept for 12 h at −90°C in the FS solutions (according to each protocol), the temperature was then raised by 5°C per hour to −45°C, rinsed in acetone and embedded in 25, 50, 75, 100% Lowicryl HM20/acetone in 2 h steps. A second 100% Lowicryl embedding for 12 h was pursued before UV polymerization for 48 h. The temperature was raised 5°C per hours until +20°C and another 48 h polymerization was conducted under UV. Sectioning was performed on a ultracut UCT from Leica Microsystem and 70 nm sections were collected in Cu/Pd slot grids coated with pioloform for ultrastructural observations. About 250 nm sections were collected similarly for tomographic purpose.

Fluorescence microscopy

CLEM Live cell imaging was performed on a Te2000u from Nikon, with 10× ELWD plan apo (NA 0.28; WD 33.5), or 40× ELWD S plan Fluor (NA 0.6; WD 3.5) mounted on a piezzo-electric, phase Ph2, GFP or Cy3 dichroic filter.

Fluorescence on sections

Lowicryl sections were imaged in distilled water on a glass slide for fluorescence imaging on the same microscope with 40× ELWD S plan Fluor (NA 0.6; WD 3.5) mounted on a piezzo-electric, phase Ph2, GFP dichroic filter for the M10-11G experiments, and with a 60× 1.4 oil DIC N2, mounted on a piezzo-electric, phase Ph2, Cy3 dichroic filter for the MNT-1 experiment.

Z-stacks of 20 µm with steps of 1.4 µm were acquired.

Electron microscopy imaging

After fluorescence on Lowicryl sections, post-contrasting 3 min of 4% uranyl acetate in H_2O plus 2 min on lead citrate was performed on all slot grids.

Electron micrographs of the HPM010 cryo-immobilized specimens were acquired on a Biotwin CM120 (Philips) Philips equipped with a bottom-mounted 1 K CCD Camera (Keen View, Olympus). Electron micrographs of the HPM100 cryo-immobilized specimens were acquired on a CM120 (Philips) Philips equipped with a side-mounted 11 MegaPixels CCD camera (Morada, Olympus) for the M10-11G experiments. For the MNT-1 experiments, electron micrographs were acquired on a Tecnai Spirit (FEI) equipped with a 4k camera CCD camera (Quemesa, Olympus).

Scanning electron microscopy

Samples were directly mounted on stubs and then gold-sputtered (Scancoat Six, Edwards). Observation was carried out with a conventional SEM operating at 15 kV (Cambridge Stereoscan S260).

Electron tomography

Tilted microscopy and electron tomography were performed on a Tecnai20 (FEI) equipped with a bottom-mounted TemCam-T416 camera (TVIPS). Images from −65 to +65 degree were acquired using TVIPS EM-MENU software and reconstruction was performed using eTomo (29).

FM/EM overlay, signal registration

Fluorescence registration was done in FIJI using TurboReg (28). The transmitted light Z stack is targeted to the low magnification electron micrograph. The saved transform is then applied to the maximum intensity Z-projection of the fluorescent channel with background removal. After color merging of the electron micrograph and the fluorescent overlay, manual adjustment of the fluorescent signal is adapted for visualization purposes. The macro is available if requested by e-mail.

Serial sections alignment

The CLEM overlays were grouped into a stack (EM/LM). Both channels were split, the serial EM sections manually aligned using MIDAS from the Imod package and the transformations were applied back to the LM stack. Both stacks were then merged back in FIJI.

Acknowledgments

We thank A.-M. Glynn for her careful proof reading and suggestions for the manuscript. We are grateful to R. Santarella-Mellwig, C. M. Casanova and S. Welsch for cell cultures and fruitful discussions around sample preparation. We thank E. M. Tranfield and C. Pugieux who provided *Xenopus laevis* CSF extracts. We are grateful to W. Kukulski for her help in applying the CLEM on sections approach in Institut Curie. We thank the Pict-IBISA from Institut Curie for strong support with the light and the electron microscopy. We thank the EMCF from EMBL for support with the preliminary EM work. We thank M. Trichet for the SEM picture. This work was supported by the EMBL PhD program, ANR MatetPro Microconnect, NIH grants R01 EY015625, ARC SL220100601359, the CNRS and 'Institut Curie'. We acknowledge France-BioImaging infrastructure supported by the French National Research Agency (ANR-10-INSB-04, ' Investments for the future ') X. H. and J. H. have invented, developed and validated the CryoCapsules and are involved in the start-up company 'CryoCapCell' that will commercialize the CryoCapsules. Contact: cryocapcell@gmail.com. X. H. conceived and, together with C. A., G. Ra., J. S. and J. H., designed the project. J. H. and X. H. designed and produced the CryoCapsules molds and adaptors. G. Re. participated in the CryoCapsule conception. X. H. conducted the experiments. S. B. did the M10 melanoma cell and HeLa cell culture for the HPM100 experiments. L. S. prepared and improved the light microscope. I. H. and C. D. helped analyzing the data. X. H. prepared the draft and C. D., I. H., J. S. and G. Ra. edited the manuscript. P. P.-G. participated in registering the images and created the script to automate the image registration on serial sections.

Supporting Information

Additional Supporting Information may be found in the online version of this article:

Figure S1: No pressure is applied to the specimen prior to the HPF shot using the CryoCapsule as compared to other CLEM approaches. Vitrification simulation with conventional tools. A) *In vitro Xenopus laevis* mitotic spindle structure deposited between substrate and covering sapphire disks (SSD, CSD) separated by a gold spacer ring (GSR) (see also Figure 1C). It is located near the X negative carbon landmark (white arrow); Cy3-Tubulin in red, Chromosome mass labeled with Hoechst. B) The assembly is loaded in the conventional HPM010 clamp between two aluminum carriers and HPF is simulated (Figure 1F). C) The sapphire assembly is recovered and re-imaged by LM. The chromosome mass (blue) has shifted, lost its structure (from a plate to a rounded shape) and the mitotic spindle structure of the Cy3-tubulin can no longer be seen (white arrow); all the fluorescent channels are electronically saturated for visualization purpose. Vitrification simulation with the CryoCapsule. D) Mitotic multipolar spindle from *X. laevis* trapped in a CryoCapsule and localized close to the positive carbon landmark (white arrow, N letter in carbon partially degraded). The chromosome mass was not labeled. E) Transfer of the CryoCapsule in the HPM010 tip and simulation of HPF. F) The CryoCapsule is recovered and re-imaged by LM. The displacement observed corresponds to the natural movements of mitotic spindles. The structure is not altered nor dismantled. Scale bar : 50 μm.

Figure S2: Specific adaptors have been designed to use the CryoCapsule with the HPM010 and the HPM100. A) The HPM010 adaptor: the CryoCapsule is deposited upside down, the covering sapphire disk facing the 200$m aluminum support membrane. The revolving part of the HPM010 clamp is folded and maintains the CryoCapsule by the plastic ring. The substrate sapphire disk faces the opened side of the clamp for a direct liquid nitrogen contact upon HPF. Both sapphire disks are 50$m thick, but for visualization purpose, the covering sapphire disk is drawn thicker. On the side of the clamp, two LN2 flow-through channels are used to help cooling the periphery of the CryoCapsule with direct liquid nitrogen contact. B) The HPM100 adaptor: the CryoCapsule is clipped upside up in the middle plate adaptor and can be directly imaged in this assembly using a long working distance objective. The covering sapphire disk is maintained in place by a ceiling lip that prevents movements and shear forces on the sample during the various HPF steps. Opened on both sides, the liquid nitrogen flows around the specimen and contact directly both sapphire disks to optimally drag the temperature of the sample down. The substrate sapphire disk is drawn thicker for visualization purpose.

Figure S3: Cooling rates of the different sub-elements usually used in high-pressure freezing of cell monolayers. A) The commonly available sapphire disks for high-pressure freezing are 50 m thick. Laser-etched sapphire disks are thicker (170 m). Thin sapphire disk has the best cooling rate of all. The aluminum carriers have a very high heat transfer (metal) and cool down very quickly. The water is the most thermo-resistant material and hence is the main limiting factor in vitrification. The heat resistance grows with the square of the thickness and should be one critical parameter to consider when proper vitrification should be achieved. Aclar®, often used to grow cells, is highly thermo-resistant. Thinness gives the vitrification properties. B) Cooling time calculation formulas: cooling time ($\theta = e2/a$), were calculated using the constants presented here and the physical formulas of thermal diffusivity: $a = (\kappa/\rho.Cp)$.

Video S1: Live cell correlative microscopy workflow: M10 Melanoma cells expressing YFP-langerin were imaged for 5 min in the CryoCapsule every 5 seconds using fluorescent and transmitted light. Just after the

last fluorescent image, the assembly, composed of the CryoCapsule and the Leica adaptor, was transferred into the HPM100 for vitrification. The samples were freeze substituted to preserve the fluorescence and serial sectioned. Each section was imaged by fluorescence and transmitted light microscopy and overlaid with the electron micrographs (430×) to map the fluorescence. Low magnification pictures were then aligned to map the fluorescence more precisely and identify the structures of interest. The live cell, fluorescence on section and EM are then aligned to illustrate the full correlative microscopy approach.

Video S2: Tutorial movie about the CryoCapsule manipulation. The covering sapphire disc in laid in the CryoCapsule in the culture petri dish. The assembly is blotted on a filter paper and clipped in the middle plate adaptor for the HPM100. The middle plate is loaded in an imaging chamber containing wet filter paper to keep the humidity high during live cell imaging. The CryoCapsule is centered above the hole of the imaging chamber to guarantee a direct light path for high quality data collection. After fluorescence live cell imaging, the sample is rapidly transferred into the HPM100 for HPF.

References

1. Hentsch D, Koch M, Spiegelhalter C, Tosch V, Kessler P, Schwab Y, Laporte J. From dynamic live cell imaging to 3D ultrastructure: novel integrated methods for high pressure freezing and correlative light-electron microscopy. PLoS One 2010 ;5:e9014.
2. Müller-Reichert T, Hohenberg H, O'Toole ET, Mcdonald KL. Cryoimmobilization and three-dimensional visualization of C. elegans ultrastructure. J Microsc 2003;212:71–80.
3. Kingdom U, Verkade P. Moving EM: the rapid transfer system as a new tool for correlative light and electron microscopy and high throughput for high-pressure freezing. J Microsc 2008;230:317–328.
4. Van Rijnsoever C, Oorschot V, Klumperman J, Rijnsoever C Van. Correlative light-electron microscopy (CLEM) combining live-cell imaging and immunolabeling of ultrathin cryosections. Cell 2008;5:973–980.
5. Nixon SJ, Webb RI, Floetenmeyer M, Schieber N, Lo HP, Parton RG. A single method for cryofixation and correlative light, electron microscopy and tomography of zebrafish embryos. Traffic 2009;10:131–136.
6. Dubochet J, Adrian M, Chang JJ, Homo JC, Lepault J, McDowall AW, Schultz P. Cryo-electron microscopy of vitrified specimens. Q Rev Biophys 1988;21:129–228.
7. Mcdonald KL. Cryopreparation methods for electron microscopy of selected model systems. Methods Cell Biol 2007;79:23–56.
8. Studer D, Michel M, Müller M. High pressure freezing comes of age. Scanning Microsc Suppl 1989;3:253–268; discussion 268–9.
9. Al-Amoudi A, Chang J, Leforestier A, McDowall AW, Salamin LM, Norlén LPO, Richter K, Blanc NS, Studer D, Dubochet J. Cryo-electron microscopy of vitreous sections. EMBO J 2004;23:3583–3588.
10. Moor H. Theory and Practice of High Pressure Freezing. Cryotechniques in Biological Electron Microscopy. 1987, pp. 175–191.
11. Leforestier A, Richter K, Livolant F, Dubochet J. Comparison of slam-freezing and high-pressure freezing effects on the DNA cholesteric liquid crystalline structure. J Microsc 1996;184:4–13.
12. Mironov AA, Polishchuk RS, Luini A. Visualizing membrane traffic in vivo by combined video fluorescence and 3D electron microscopy. Trends Cell Biol 2000;10:349–353.
13. Studer D, Graber W, Al-Amoudi A, Eggli P. A new approach for cryofixation by high-pressure freezing. J Microsc 2001;203:285–294.
14. Mcdonald KL, Morphew M, Verkade P, Müller-Reichert T. Recent advances in high-pressure freezing: equipment- and specimen-loading methods. Methods Mol Biol 2007;369:143–173.
15. Hawes P, Netherton CL, Mueller M, Wileman T, Monaghan P, Road A. Rapid freeze-substitution preserves membranes in high-pressure frozen tissue culture cells. J Microsc 2007;226:182–189.
16. Salmon ED, Goode D, Maugel TK, Bonar DB. Pressure-induced depolymerization of spindle microtubules. III. Differential stability in HeLa cells. J Cell Biol 1976;69:443–454.
17. Lenormand C, Spiegelhalter C, Cinquin B, Bardin S, Bausinger H, Angénieux C, Eckly A, Proamer F, Wall D, Lich B, Tourne S, Hanau D, Schwab Y, Salamero J, de la Salle H. Birbeck granule-like organized smooth endoplasmic reticulum resulting from the expression of a cytoplasmic YFP-tagged langerin. PLoS One 2013;8:e60813.
18. Delevoye C, Hurbain I, Tenza D, Sibarita J, Uzan-Gafsou S, Ohno H, Geerts WJC, Verkleij AJ, Salamero J, Marks MS, Raposo G. AP-1 and KIF13A coordinate endosomal sorting and positioning during melanosome biogenesis. J Cell Biol 2009;187:247–264.
19. Giboz J, Copponnex T, Patrice M, Mélé P. Microinjection molding of thermoplastic polymers: a review. J Micromech Microeng 2007;17:R96–R109.
20. Mankidy R, Wiseman S, Ma H, Giesy JP. Biological impact of phthalates. Toxicol Lett 2013;217:50–58.
21. Jiménez N, Van Donselaar EG, De Winter DAM, Vocking K, Verkleij AJ, Post JA, Donselaar EGVAN. Gridded Aclar: preparation methods and use for correlative light and electron microscopy of cell monolayers, by TEM and FIB-SEM. J Microsc 2010;237:208–220.
22. Jiménez N, Humbel BM, van Donselaar E, Verkleij AJ, Burger KNJ. Aclar discs: a versatile substrate for routine high-pressure freezing of mammalian cell monolayers. J Microsc 2006;221:216–223.
23. Mcdonald KL, Schwarz H, Thomas M, Müller-Reichert T, Webb R, Buser C, Morphew M. Tips and tricks for high-pressure freezing of model systems. Methods Cell Biol 2010;96:671–693.
24. Moor H, Bellin G, Sandri C, Akert K. The influence of high pressure freezing on mammalian nerve tissue. Cell Tissue Res 1980;209:201–216.
25. Guizetti J, Mäntler J, Müller-Reichert T, Gerlich DW. Correlative time-lapse imaging and electron microscopy to study abscission in HeLa cells. Methods Cell Biol 2010;96:591–601.
26. Kukulski W, Schorb M, Kaksonen M, Briggs JAG. Plasma membrane reshaping during endocytosis is revealed by time-resolved electron tomography. Cell 2012;150:508–520.
27. Kukulski W, Schorb M, Welsch S, Picco A, Kaksonen M, Briggs JAG. Correlated fluorescence and 3D electron microscopy with high sensitivity and spatial precision. J Cell Biol 2011;192:111–119.
28. Thévenaz P, Ruttimann UE, Unser M. A pyramid approach to subpixel registration based on intensity. IEEE Trans Image Process 1998;7:27–41.

29. Kremer JR, Mastronarde DN, McIntosh JR. Computer visualization of three-dimensional image data using IMOD. J Struct Biol 1996;116:71–76.
30. Karreman MA, Agronskaia AV, van Donselaar EG, Vocking K, Fereidouni F, Humbel BM, Verrips CT, Verkleij AJ, Gerritsen HC. Optimizing immuno-labeling for correlative fluorescence and electron microscopy on a single specimen. J Struct Biol 2012;180: 382–386.
31. Müller-Reichert T, Srayko M, Hyman AA, O'Toole ET, Mcdonald KL. Correlative light and electron microscopy of early Caenorhabditis elegans embryos in mitosis. Methods Cell Biol 2007;79:101–119.
32. Dubochet J, Sartori Blanc N. The cell in absence of aggregation artifacts. Micron 2001;32:91–99.
33. Matias VRF, Al-Amoudi A, Dubochet J, Beveridge TJ. Cryo-transmission electron microscopy of frozen-hydrated sections of Escherichia coli and Pseudomonas aeruginosa. J Bacteriol 2003;185:6112–6118.
34. Brown E, Van Weering J, Sharp T, Mantell J, Verkade P. Capturing endocytic segregation events with HPF-CLEM. Methods Cell Biol 2012;111:175–201.
35. Betzig E, Patterson GH, Sougrat R, Lindwasser OW, Olenych S, Bonifacino JS, Davidson MW, Lippincott-Schwartz J, Hess HF. Imaging intracellular fluorescent proteins at nanometer resolution. Science 2006;313:1642–1645.
36. Desai A, Murray A, Mitchison TJ, Walczak CE. The use of Xenopus egg extracts to study mitotic spindle assembly and function in vitro. Methods Cell Biol 1999;61:385–412.